Elsevier Editorial System(tm) for International Journal of Impact Engineering
Manuscript Draft

Manuscript Number:

Title: Pressure-impulse diagram of a beam developing non-linear membrane action under blast loading

Article Type: Original Research Paper

Keywords: pressure-impulse diagram; blast loading; non-linear membrane force; lateral restraint; lateral inertia; M-N interaction.

Corresponding Author: Prof. Vincent Denoel,

Corresponding Author's Institution:

First Author: Lotfi Hamra

Order of Authors: Lotfi Hamra; Jean-François Demonceau; Vincent Denoel

Abstract: The p-I diagram of a frame beam subjected to blast loading is established, including the elastic lateral restraint and inertia offered by the rest of the structure, the development of nonlinear membrane action and also, the bending-tension (M-N) interaction that develops in the plastic hinges. The analytical procedures to compute the asymptotes in the p-I diagram as well as a parametric study on the p-I diagram are provided. A dimensional analysis of the problem reveals that, under the considered assumptions, four dimensionless parameters mainly influence the required ductility of the beam. Two of them are related to the behaviour of the indirectly affected part (the lateral restraint and mass). Another one is related to the mechanical properties of the investigated beam (i.e. the ratio of the bending to axial resistance). The last parameter incorporates scales of the geometry and of the deformed configuration at the onset of the plastic mechanism.

Cover Letter

University of Liège, Faculty of Applied Sciences
Department of Architecture, Geology, Environment and Constructions

Vincent Denoël, Associate Professor

Université de Liège

ArGEnCo

To: **International Journal of Impact Engineering**
Ed. Dr. M. Langseth

Liège, December 1st, 2014.

OBJECT: Paper submission to International Journal of Impact Engineering

Dear Dr. Langseth,

Please consider this submission as an interesting potential paper for the **International Journal of Impact Engineering**.

We hope this paper will be received with much interest by the readers of your Journal. We also hope it will be received with a positive review, with the examination level corresponding to your standards.

We wish to warmly acknowledge the attention that the Edition team and Referees will pay to this submission.

Yours sincerely,

Prof. V. Denoël

University of Liège, Structural Engineering Divsion (SE)
Institut Mécanique – Génie Civil BAT B52/3
Chemin des Chevreuils, 1 B-4000 Liège (Belgium)
Tel. ++ 32 (0)4 366 29 30 Fax. ++ 32 (0) 4 366 95 34 Parking P52
Email : V.Denoel@ulg.ac.be www.argenco.ulg.ac.be/SE

Pressure-impulse diagram of a beam developing non-linear membrane action under blast loading

L. Hamra[a,*], J.-F. Demonceau[a], V. Denoël[b]

[a] *University of Liège, Department of Architecture, Geology, Environment and Constructions, Mechanics of Solids and Structures, Chemin des Chevreuils, 1, B52/3, 4000 Liège, Belgium*
[b] *University of Liège, Department of Architecture, Geology, Environment and Constructions, Structural Engineering Division, Chemin des Chevreuils, 1, B52/3, 4000 Liège, Belgium*

Abstract

The p-I diagram of a frame beam subjected to blast loading is established, including the elastic lateral restraint and inertia offered by the rest of the structure, the development of nonlinear membrane action and also, the bending-tension (M-N) interaction that develops in the plastic hinges. The analytical procedures to compute the asymptotes in the p-I diagram as well as a parametric study on the p-I diagram are provided. A dimensional analysis of the problem reveals that, under the considered assumptions, four dimensionless parameters mainly influence the required ductility of the beam. Two of them are related to the behaviour of the indirectly affected part (the lateral restraint and mass). Another one is related to the mechanical properties of the investigated beam (i.e. the ratio of the bending to axial resistance). The last parameter incorporates scales of the geometry and of the deformed configuration at the onset of the plastic mechanism.

Keywords: pressure-impulse diagram, blast loading, non-linear membrane force, lateral restraint, lateral inertia, M-N interaction.

PACS: xxx.xxx, xxx.xxx, xxx.xxx

2008 MSC: xxx.xxx

Highlights:

- An analytical model to predict the response of a frame beam subjected to blast loading is proposed.
- The lateral restraint may significantly reduce the required ductility at the beam level.
- The M-N interaction developing in the yielded zone increases the required ductility at the beam level.

1. Introduction

Recent standards or norms are concerned about the need to confer robustness to structures subjected to exceptional events such as natural catastrophes, explosions or impacts, in order to avoid their progressive collapse. In particular it is expected that the loss of any column in a frame building results in a possibly highly damaged but still stable structural system. An accurate finite element modeling of all possible scenarii is by far too expensive and simpler analysis tools are required, at least at early design stages. Driven by the recent observations that the structural behaviour of the beam above a compartment affected by a blast mainly governs the local response [1, 2], a simple model of the system is developed with a condensation of the rest of the structure, usually referred to as the *indirectly affected part* (IAP). More precisely, this paper focuses on the determination of the required ductility

*Corresponding author
Email addresses: lhamra@ulg.ac.be (L. Hamra), jfdemonceau@ulg.ac.be (J.-F. Demonceau), v.denoel@ulg.ac.be (V. Denoël)

of frame beams subjected to a blast loading considering the effects of lateral inertia and elastic restraint offered by the IAP.

The pressure-impulse (p-I) diagram is commonly used to design elements or structures for a given blast loading. It consists of contour sets of damage for structural elements [3, 4, 5]. The damage index could be the required ductility for beams or slabs in bending [6], the ratio of the residual to the design axial resistances for columns [7] or the ultimate rotation for joints [8].

The typical profile of a p-I diagram is composed of two asymptotes pertaining to the fast (impulsive) and the slow (quasi-static) dynamics. The transition between these two extremes corresponds to a dynamic regime, where the duration of the loading interacts with the timescales of the structure.

In the literature, the conversion of a continuous beam to an equivalent single degree of freedom (SDOF) system is suggested in order to assess the required ductility of the beam or eventually to develop its corresponding p-I diagram. The mass, the stiffness and the load applied on the beam are multiplied by some lumping factors assuming a flexural behaviour of the beam [3, 4, 5, 6]. However, the effects of shear and membrane forces are neglected although they can be significant in some cases [9, 10, 11, 12, 13].

R.Vaziri et Al. [14] and N.Jones [9] looked into the development of the membrane force and the M-N interaction for a simply supported or fixed beam. Langdon and Schleyer [15] presented a model of a beam including some lateral and rotational restraints at its ends as well as the development of the membrane force. They compared the response of the model with the experimental results of the post-critical response of a corrugated steel wall panel subjected to blast loading. Fallah and Louca [16] derived a p-I diagram for equivalent softening and hardening SDOF models substituting the structural behaviour of the corrugated steel wall by an equivalent bilinear resistance-displacement curve. They also propose analytical equations of the asymptotes expressed as a function of the so-called hardening/softening index.

Dragos and Wu have recently proposed a full analytical procedure based on an empirical approach to derive the p-I diagram of a bilinear SDOF model [17]

The aim of this paper is to establish the p-I diagram of a frame beam subjected to a close-field local internal blast loading including the effect of nonlinear membrane actions, the bending moment-axial (M-N) plastic resistance interaction curve of the beam as well as the dynamic interaction with the reduced model of the IAP of the structure. An inexpensive iterative analytical scheme is derived for the expressions of the p-I diagram asymptotes and a dimensionless parametric study according to four structural variables is also performed.

2. Problem Formulation

2.1. Description of the problem

The considered problem consists in the establishment of the structural dynamic response of a beam under a uniformly distributed blast loading $p(x,t)$, see Figure 1. The beam has a length 2ℓ and is characterized by a lineic

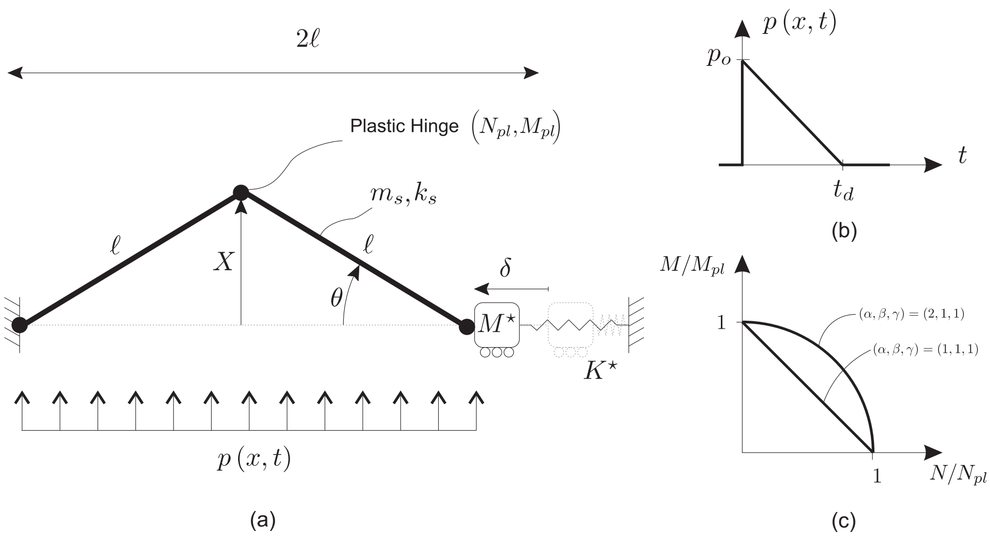

Figure 1: (a) Sketch of the considered problem, (b) Idealized blast loading, (c) Axial force-bending moment interaction law

mass m_s and an equivalent elastic bending stiffness k_s. Specific to this problem is the lateral restraint $K^\star$ and the mass $M^\star$ that materialize a horizontal restraint as well as a participating mass; they model the passive interaction of this beam with the IAP and result from a dynamic condensation as stated in Section 2.2. The loading is assumed to develop synchronously along the beam and is idealized as a triangular pulse, see Fig. 1-b, so that

$$p(x,t) = p_o \left(1 - \frac{t}{t_d}\right) \tag{1}$$

where t represents the time variable, p_o is the peak blast pressure and t_d is the positive phase duration. The momentum I associated with this pressure field is thus given by

$$I = \frac{p_o t_d}{2} \ell. \tag{2}$$

Consistently with common practice in impact engineering, the loading is parametrized by (p_o, I) in the sequel, rather than (p_o, t_d). The maximum response of the beam under this parametric blast loading is then represented in a (p_o, I) diagram for various blast durations and intensities.

The beam deforms symmetrically under this loading. The material law is elastic perfectly plastic but, in order to simplify the kinematics, the deflection in the elastic regime is neglected so that the deformed configuration of the beam, after plasticity has installed, consists of two straight elastic portions connected by a plastic hinge. Two additional plastic hinges also develop at the end supports of the beam. The kinematics are thus fully described by the mid-span displacement X or equivalently by the rotation $\theta = X/\ell$ of each portion of the beam, which makes this model that of a single degree-of-freedom system.

The presence of the lateral restraint and mass generates membrane (axial) forces in the beam. They are captured in the model thanks to a second-order large displacement/small rotation model, writing the equilibrium equations in the deformed configuration but yet assuming moderate rotations, i.e. keeping second order terms as

$$\begin{aligned}\sin\theta \simeq \tan\theta &\simeq \theta = \frac{X}{\ell}\\ \cos\theta &\simeq 1-\frac{\theta^2}{2} = 1-\frac{X^2}{2\ell^2}\end{aligned} \tag{3}$$

so that the elongation of the lateral spring reads

$$\delta = 2\ell\left(1-\cos\theta\right) = \frac{X^2}{\ell}. \tag{4}$$

Using an overhead dot to indicate differentiation with respect to time t, the shortening velocity and acceleration of the chord thus read

$$\dot{\delta} = \frac{2}{\ell}X\dot{X} \quad ; \quad \ddot{\delta} = \frac{2}{\ell}\left(\dot{X}^2 + X\ddot{X}\right). \tag{5}$$

Because of the membrane force $K^\star\delta$ increasing quadratically in the lateral spring as the transverse displacement X increases, the plastic bending moment M_{pl} that could, otherwise, be beared by the plastic hinge might drop during blasting. Accordingly the model presented next incorporates the $M-N$ interaction law between the bending moment M and the axial force N into the beam, which might be reduced on an inclusive basis in order to account for some partially resistant connections. For the sake of generality in the developments, the considered interaction law is

$$\left(\frac{M}{M_{pl}}\right)^\beta + \gamma\left(\frac{N}{N_{pl}}\right)^\alpha = 1 \tag{6}$$

where N_{pl} is the plastic axial resistance. Symbols α, β and γ refer to some parameters of the model (Fig. 1-c), which should be selected in accordance with the considered application. They might take on different values depending on the constitutive material in the structure, namely involving steel, concrete or composite structures ([18, 19, 20, 21, 22]).

The main assumptions of the model are that: (i) the lateral restraint (and the IAP) remain(s) in an elastic regime; (ii) the beam-to-column joints are perfectly rigid; (iii) the axial elongation of the plastic hinges under bending moment and membrane forces and the elastic elongation of the beam are neglected; (iv) the material law is elastic perfectly plastic; ; (v) the effect of the strain rate on the resistance is not considered ; (vi) the position of the plastic hinges is fixed and (vii) the shear failure is not considered.

2.2. Extraction of the beam from the structure

This section discusses the extraction of the beam from the whole structure in order to study the simplest configuration represented in Figure 1. The main challenge of dynamic condensation is to reproduce the important dynamic signature of the global finite element model after reduction of the IAP of the structure to a lateral equivalent mass and spring. No unique solution exists; some are discussed in this Section and illustrated in the applications.

In a finite element context, the equation of motion of the structure reads

$$\mathbf{M}_{str}\ddot{\mathbf{X}}_{str} + \mathbf{f}_{int}\left(\mathbf{X}_{str}\right) = \mathbf{P}_{str} \tag{7}$$

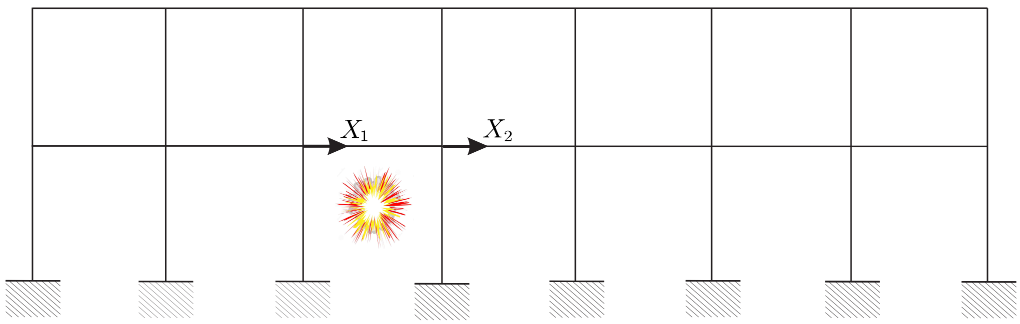

Figure 2: Horizontal displacements at the ends of the blast loaded beam.

where $\mathbf{M}_{str}$, $\mathbf{f}_{int}$, $\mathbf{X}_{str} = \begin{bmatrix} X_1 & X_2 & \mathbf{X}_R \end{bmatrix}^T$ and $\mathbf{P}_{str}$ respectively represent the mass matrix, the internal forces, the nodal displacements (see Figure 2) and the dynamic external loading.

In order to simplify the model reduction, we assume that the blast loading instantaneously annihilates the bending stiffness at the connection of the investigated beam and its supporting columns. However, the vertical reaction still exists since the columns are supposed to be still stable after explosion, meaning that the residual axial plastic resistance of them are at least 1.25 higher than the vertical load [7]. The internal forces can be decomposed into two parts

$$\mathbf{M}_{str} \begin{bmatrix} \ddot{X}_1 \\ \ddot{X}_2 \\ \ddot{\mathbf{X}}_R \end{bmatrix} + \mathbf{K}_{str} \begin{bmatrix} X_1 \\ X_2 \\ \mathbf{X}_R \end{bmatrix} + \phi\left(X_1 - X_2; p\right) \begin{bmatrix} 1 \\ -1 \\ 0 \end{bmatrix} = 0, \tag{8}$$

namely the elastic restoring forces in the structure, expressed in terms of the stiffness matrix $\mathbf{K}_{str}$ and the auto-balanced membrane forces $\phi\left(X_1 - X_2; p\right)$ associated with the kinematic quantities X_1 and X_2 corresponding to the horizontal displacements of the ends of the beam.

The change of variables

$$\boldsymbol{\Delta}_{str} := \begin{bmatrix} \delta \\ X_h \\ \mathbf{X}_R \end{bmatrix} = \begin{bmatrix} X_1 - X_2 \\ X_1 + X_2 \\ \mathbf{X}_R \end{bmatrix} = \begin{bmatrix} 1 & -1 & 0 \\ 1 & 1 & 0 \\ 0 & 0 & \mathbf{I} \end{bmatrix} \mathbf{X}_{str} \Longleftrightarrow \mathbf{X}_{str} = \begin{bmatrix} \frac{1}{2} & \frac{1}{2} & 0 \\ -\frac{1}{2} & \frac{1}{2} & 0 \\ 0 & 0 & \mathbf{I} \end{bmatrix} \boldsymbol{\Delta}_{str} := \mathbf{T}\boldsymbol{\Delta}_{str} \tag{9}$$

explicitly introduces the relative elongation $X_1 - X_2$.

Substitution of (9) into (8) and multiplication by $\mathbf{T}^T$ projects the equation of motion in a new coordinate system composed of the chord elongation of the beam δ, the average horizontal displacement X_h and the displacements of the other nodes of the model. It reads

$$\mathbf{M}_{str,T}\ddot{\mathbf{\Delta}}_{str} + \mathbf{K}_{str,T}\mathbf{\Delta}_{str} = -\phi\left(\delta;p\right)\begin{bmatrix}1\\0\\0\end{bmatrix} \tag{10}$$

where $\mathbf{M}_{str,T} = \mathbf{T}^T\mathbf{M}_{str}\mathbf{T}$ and $\mathbf{K}_{str,T} = \mathbf{T}^T\mathbf{K}_{str}\mathbf{T}$. We may now recourse to known model reduction techniques in order to lump this dynamical system to the single degree-of-freedom δ. These techniques assume that the lumped degrees-of-freedom are expressed as an affine transformation of the master degree-of-freedom δ ,

$$\mathbf{\Delta}_{str} = \mathbf{T}^*\delta, \tag{11}$$

where $\mathbf{T}^*$ is a transformation matrix, selected in accordance with the type of the model reduction. After reduction, the scalar governing equation reads

$$M^*\ddot{\delta} + K^*\delta = -\phi(\delta;p) \tag{12}$$

where $M^* = \mathbf{T}^{*T}\mathbf{M}_{str,T}\mathbf{T}^*$ and $K^* = \mathbf{T}^{*T}\mathbf{K}_{str,T}\mathbf{T}^*$. The hypothesis (11) could look rather strong, at first sight, as it enforces all degrees-of-freedom, and among others the average horizontal displacement of the beam, to evolve synchronously with the reduced coordinate δ. Model reduction techniques may however preserve an accurate quasi-static response (Guyan) or oscillatory response in a vibration mode of the structure (all the responses vibrate in phase and their amplitude are defined to within a constant), as seen below with four different examples of reduction.

First, a classical procedure to reduce a finite element model is the Guyan (or static) condensation [23]. The set of equations (10), disregarding inertia terms, is described by

$$\mathbf{K}_{str,T}\begin{bmatrix}\delta\\ \mathbf{\Delta}_R\end{bmatrix} = -\phi\left(\delta;p\right)\begin{bmatrix}1\\ \mathbf{0}\end{bmatrix} \tag{13}$$

where $\mathbf{K}_{str,T} = \begin{bmatrix}K_{\delta\delta} & \mathbf{K}_{\delta R}\\ \mathbf{K}_{R\delta} & \mathbf{K}_{RR}\end{bmatrix}$ and where $\mathbf{\Delta}_R = \begin{bmatrix}X_h\\ \mathbf{X}_R\end{bmatrix}$ gathers the degrees-of-freedom to be condensed. As a result , they can be expressed as

$$\mathbf{\Delta}_R = \left(-\mathbf{K}_{RR}^{-1}\mathbf{K}_{R\delta}\right)\delta \tag{14}$$

and the Guyan transformation is finally given by

$$\mathbf{T}_G^* = \begin{bmatrix}1\\ \left(-\mathbf{K}_{RR}^{-1}\mathbf{K}_{R\delta}\right)\end{bmatrix}. \tag{15}$$

Second, the Improved Reduced System (IRS) reduction process adjusts the Guyan condensation by adding some corrective terms in order to better represent the mass associated with the discarded degrees-of-freedom [24]. The IRS transformation is given by

$$\mathbf{T}^{*}_{IRS} = \mathbf{T}^{*}_{G} + \mathbf{S}\mathbf{M}_{str,T}\mathbf{T}^{*}_{G}M^{*-1}_{G}K^{*}_{G} \tag{16}$$

where $\mathbf{M}_{str,T} = \begin{bmatrix} M_{\delta\delta} & \mathbf{M}_{\delta R} \\ \mathbf{M}_{R\delta} & \mathbf{M}_{RR} \end{bmatrix}$, $\mathbf{S} = \begin{bmatrix} 0 & 0 \\ 0 & \mathbf{K}^{-1}_{RR} \end{bmatrix}$, M^{*}_{G} and K^{*}_{G} are the reduced mass and stiffness resulting from the Guyan condensation. This process is known to improve the accuracy of the results obtained from the Guyan condensation for higher modes of the system.

Third, if the global model vibrates mainly according to one mode shape, a dynamic condensation selecting that mode shape as a basis for the transformation matrix $\mathbf{T}^{*}$ is more appropriate as it conserves one eigen mode and eigenvalue of the original model[25]. For the simple degree-of-freedom condensation under consideration here, the transformation matrix is readily obtained as

$$\mathbf{T}^{*}_{D} = \begin{bmatrix} 1 \\ \left(-\left(\mathbf{K}_{RR} - \omega^{2}\mathbf{M}_{RR}\right)^{-1}\left(\mathbf{K}_{R\delta} - \omega^{2}\mathbf{M}_{R\delta}\right)\right) \end{bmatrix} \tag{17}$$

where ω represents the natural frequency of the eigen mode of interest.

The System Equivalent Reduction Expansion Process (SEREP) [26] is a fourth method that preserves several natural frequencies of the global model . The eigen solution of the reduced system is exact and does not depend on the location nor the number of points preserved in the reduced model. As only one degree-of-freedom is kept in the current approach, the SEREP provides a solution very similar to that given by the dynamic condensation as the natural frequency is the same but the reduced stiffness and mass can be slightly different in some cases.

Later in this paper, one of these reduction models is shown to be more appropriate, and thus, that last one is selected to present all our numerical results.

2.3. Structural Behaviour

The structural behaviour of the equivalent single degree-of-freedom oscillator is sketched in Figure 3. It illustrates, under a blast loading, the total internal force F_{int} in the nonlinear oscillator as a function of the generalized coordinate X. It is composed of the internal forces in the beam resulting from the elastic-platic deformations and of the nonlinear restoring forces in the horizontal spring. This illustration is provided qualitatively here, while the equivalence between the continuous structure depicted in Fig. 1-a and this single degree-of-freedom oscillator is formally developed later, based on an energy equivalence and displacement-based approach. Figure 3-c shows the free body diagram of the equivalent oscillator, indicating the balance of internal forces F_{int}, external forces F_{ext} and inertial forces $M_s\ddot{X} + F_{inert}\left(M^{*}\ddot{\delta}\right)$ where M_s is a generalized mass, as discussed later.

After a linear elastic regime extending to a yield displacement $X_y = \frac{M_p l^2}{3EI_b}$ (where I_b and E are the inertia of the beam and the Young's modulus of the material), the elastic strain energy stored in the system is U_1. This energy is

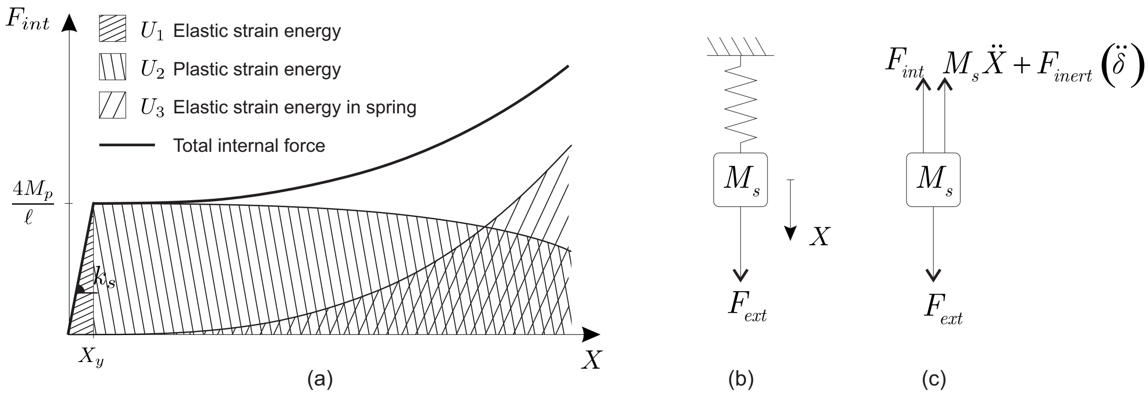

Figure 3: (a) Sketch of the structural behaviour of the equivalent single degree-of-freedom oscillator, (b) equivalent single degree-of-freedom oscillator, (c) free body diagram of the equivalent oscillator.

recovered in a reversible manner during the unloading regime. Although there is a slight shift in their occurrence, it is assumed that all three plastic hinges of the problem form at the same time, after the mid-span displacement has reached X_y and for a distributed pressure p_s equal to $\frac{4M_p}{\ell^2}$ corresponding, actually, to occurrence of the third plastic hinge. The secant stiffness in the elastic regime is thus $k_s = \frac{p_s l}{X_y} = \frac{12EI_b}{l^3}$.

After yielding has occurred, the beam enters a dissipative plastic regime where some strain energy U_2 is dissipated in the plastic hinges. In an elastic-perfectly plastic model, one would expect a horizontal plateau associated with the plastic bending moment in the plastic hinges. However, the maximum allowable bending moment accepted by the plastic hinges is initially M_p but this value is more or less rapidly affected —depending on the spring stiffness $K^\star$ and the mass M^*— as the axial force in the beam grows. It then features a smooth and gentle decrease, as seen in Fig. 3-a, as membrane forces develop. Notice they might be estimated as follows. We consider that the plastic hinges have already developed at that stage, i.e. the shear force in the beam is equal to $2M(N)/\ell$ where $M(N)$ represents the reduced allowable bending moment, as per the interaction law (see Equation (6)). It can be approximated by $2M_{pl}/l$ as the dissipation of energy in the beam will be overestimated. The axial force in the beam is obtained by the horizontal equilibrium equation at the right end of the beam

$$\begin{aligned} N &\simeq -\phi(\delta;p) + \frac{2M_{pl}}{\ell}\frac{X}{\ell} \\ &\simeq \frac{2}{\ell}\left[\left(\dot{X}^2 + X\ddot{X}\right)M^\star + \frac{X^2}{2}K^\star + M_{pl}\frac{X}{\ell}\right]. \end{aligned} \tag{18}$$

At last but not least, internal forces in the equivalent single degree-of-freedom system are also composed of the elastic restoring force in the lateral spring. These grow proportional to the third power of the transverse displacement of the beam.

2.4. Governing Equations

Energy conservation states that the sum of kinetic energy K and elastic-plastic strain energy $U = U_1 + U_2 + U_3$ is equal to the work done by the external forces

$$K + U_1 + U_2 + U_3 = W. \tag{19}$$

The elastic energy U_1 stored in the beam is given by

$$U_1 = \frac{1}{2} k_s X^2 \tag{20}$$

where k_s is the equivalent elastic bending stiffness of the beam, see Figure 3. This expression is valid for $X \in [0; X_y]$ and should be set equal to $\frac{1}{2} k_s X_y^2$ for values of X out of this interval. Taking into account the reduction of the maximum allowable bending moment, the energy dissipated in the plastic hinges is equal to zero for $X \in [0; X_y]$ and expressed as

$$U_2 = 4 \int_{X_y/\ell}^{X/\ell} M \left[N\left(\theta, \dot{\theta}, \ddot{\theta}\right) \right] d\theta = \frac{4}{\ell} \int_{X_y}^{X} M \left[N\left(\frac{\mathcal{X}}{\ell}, \frac{\dot{\mathcal{X}}}{\ell}, \frac{\ddot{\mathcal{X}}}{\ell} \right) \right] d\mathcal{X} \tag{21}$$

for $X \geq X_y$ and $\dot{X} \geq 0$. Since we mainly focus on the determination of the maximum displacement and internal forces, the configurations corresponding to the quadrants $\left(X, \dot{X}\right) \in [X_y; +\infty] \times [-\infty; 0]$ or $\left(X, \dot{X}\right) \in [-\infty; 0] \times \mathbb{R}$ are of secondary importance and are not developed in this paper. Third, the energy stored in the lateral spring is given by

$$U_3 = \int_0^{\delta} K^\star \Delta \, d\Delta = \int_0^{X} K^\star \frac{\mathcal{X}^2}{\ell} \frac{2\mathcal{X}}{\ell} \, d\mathcal{X} = \frac{1}{2} K^\star X^2 \frac{X^2}{\ell^2}. \tag{22}$$

The total kinetic energy reads

$$K = \frac{1}{2} M_s \dot{X}^2 + \frac{1}{2} M^\star \dot{\delta}^2 = \frac{1}{2} \left(M_s + 4 M^\star \frac{X^2}{\ell^2} \right) \dot{X}^2 \tag{23}$$

where $M_s = 2 m_s \ell / 3$ is the generalized mass corresponding to the assumed kinematics.

The external work done by the blast loading is given by

$$W = 2 \int_0^{\ell} \int_0^{X} p \left(1 - \frac{x}{\ell} \right) d\mathcal{X} dx = 2 \int_0^{\ell} p X \left(1 - \frac{x}{\ell} \right) dx = p \ell X \tag{24}$$

so that, finally, the energy conservation reads

$$\frac{1}{2} \left(M_s + 4 M^\star \frac{X^2}{\ell^2} \right) \dot{X}^2 + U_{int,b} + \frac{1}{2} K^\star X^2 \frac{X^2}{\ell^2} = p \ell X \tag{25}$$

with

$$U_{int,b} = \begin{cases} \frac{1}{2} k_s X^2 & \text{for } X \leq X_y, \\ \frac{1}{2} k_s X_y^2 + \frac{4}{\ell} \int_{X_y}^{X} M \left[N\left(\mathcal{X}, \dot{\mathcal{X}}, \ddot{\mathcal{X}} \right) \right] d\mathcal{X} & \text{for } X > X_y \text{ and } \dot{X} \geq 0. \end{cases} \tag{26}$$

2.5. Equation of Motion

The equation of motion of the generalized problem is derived by differentiating the energy conservation law with respect to time and then dividing this conservation of power by the velocity $\dot{X}$.

The first term of the equation (25) provides the inertial force of the beam

$$\frac{1}{\dot{X}}\frac{dK}{dt} = \left(M_s + 4M^\star \frac{X^2}{\ell}\right)\ddot{X} + 4M^\star \frac{X\dot{X}^2}{\ell^2} \tag{27}$$

The time derivative of the strain energy induced in the beam gives

$$F_{int,b} := \frac{1}{\dot{X}}\frac{dU_{int,b}}{dt} = \begin{cases} k_s X & \text{for } X \leq X_y, \\ \frac{4}{\ell}M\left[N\left(X,\dot{X},\ddot{X}\right)\right] & \text{for } X > X_y \text{ and } \dot{X} \geq 0 \end{cases} \tag{28}$$

where $F_{int,b}\,(t)$ is the equivalent internal force in the beam.

The third term of equation (25) provides the force in the lateral restraint

$$F_{int,K} := \frac{1}{\dot{X}}\frac{dU_3}{dt} = 2K^\star \frac{X^3}{\ell^2} \tag{29}$$

where $F_{int,K}\,(t)$ is the equivalent internal force in the lateral restraint. Finally, the term associated with the external force due provides

$$F_{ext} = \frac{1}{\dot{X}}\frac{dW}{dt} = p\ell \tag{30}$$

where $F_{ext}\,(t)$ is the equivalent force due to blast loading.

All in all, the equation of motion reads

$$\left(M_s + 4M^\star \frac{X^2}{\ell}\right)\ddot{X} + 4M^\star \frac{X\dot{X}^2}{\ell^2} + F_{int,b}\left(X,\dot{X},\ddot{X}\right) + 2K^\star \frac{X^3}{\ell^2} = p\ell \tag{31}$$

This is the nonlinear equation (with time-varying mass) that needs to be solved in order to determine the maximum displacement, and so the required ductility, of the system.

2.6. Scaling and Dimensionless Formulation

A natural timescale of the problem is the characteristic period of the elastic beam without lateral restraint and inertia $T = \sqrt{M_s/k_s}$. The characteristic pessure $p_s = 4M_{pl}/\ell^2$ corresponds to the the static pressure at which the plastic beam mechanism is formed, while the characteristic displacement definitely corresponds to the yield displacement $X_y = p_s\ell/k_s$. The dimensionless version of the equation of motion is obtained by rescaling the time by the characteristic time, and dividing both sides of the equation of motion by the characteristic force $k_s X_y = p_s\ell$

$$\left(1 + \psi_M \theta_y^2 \overline{X}^2\right)\overline{X}'' + \psi_M \theta_y^2 \overline{X}\,\overline{X}'^2 + \overline{F}_{int,b}\left(\overline{X},\overline{X}',\overline{X}''\right) + 2\psi_K \theta_y^2 \overline{X}^3 = \overline{p}\left(1 - \frac{\tau}{\tau_d}\right) \tag{32}$$

where $\overline{X} = X/X_y$ is the dimensionless displacement and the prime symbol ' represents differentiation with respect to the dimensionless time $\tau = t/T$. Other dimensionless parameters of the problem naturally appear as the ratio $\tau_d = t_d/T$ of the duration of blasting over the characteristic timescale, the ratio $\psi_M = 4M^\star/M_s$ of the lateral participating mass to the mass of the beam, the ratio $\psi_K = K^*/K_s$ of the lateral restraint to the stiffness of the beam, the yield rotation $\theta_y = X_y/\ell$, the dimensionless peak overpressure of the blast loading $\overline{p} = p_0/p_s$ and the dimensionless internal forces defined as

$$\overline{F}_{int,b} = \frac{F_{int,b}}{p_s \ell} = \begin{cases} \overline{X} & \text{for } \overline{X} \leq 1, \\ m\left[n\left(\overline{X}, \overline{X}', \overline{X}''\right)\right] & \text{for } \overline{X} > 1 \text{ and } \overline{X}' \geq 0. \end{cases} \tag{33}$$

The dimensionless axial force $n := N/N_{pl}$ and its interaction with the dimensionless bending moment $m := M/M_{pl}$ are respectively given by

$$n = 4\xi\theta_y \overline{X} + 8\xi\theta_y\psi_K \overline{X}^2 + 4\psi_M\xi\theta_y \left(\overline{X}'^2 + \overline{X}\,\overline{X}''\right) \tag{34}$$

$$m^\beta + \gamma n^\alpha = 1 \tag{35}$$

where $\xi = (M_{pl}/2\ell)/N_{pl}$ is the ratio of bending to axial strengths. The demand in ductility

$$\mu = \max_{t \in \mathbb{R}^+} \overline{X}(t) = \frac{X_m}{X_y}, \tag{36}$$

where X_m represents the maximum displacement of the beam, is only ruled out by the six dimensionless numbers of this problem, namely $\psi_K, \psi_M,\ \xi, \theta_y,\ \bar{p}, \tau_d$.

The scope of this work is to analyse how the demand of ductility μ is related to these parameters. There is no closed-form solution of the governing equation of the problem (32), taking into account (33) and (34)-(35). We will therefore limit the study to the influence of the problem parameters on the demand in ductility. As the influence of some parameters such as the duration of the blasting are relatively well understood, we mainly focus on the influence of ψ_K and ψ_M as they are specific to this model.

For the protection of staff and equipment through the attenuation of blast pressure and to shield them from the effects of fragments and falling portions of the structure, recommended deformation limits are given under category 1 in Table 1. For the protection of structural elements themselves from collapse under the action of blast loading, the recommended deformation limits are given under protection category 2 in Table 1 [5].

The dimensionless parameters ψ_K and ψ_M depend, respectively, on the stiffness and the inertia offered by the IAP and result from reduction models. In Figure 4-a, the structure has no lateral restraint nor additionnal inertia because, as explained earlier, the bending stiffness of the columns is neglected and the weight of the columns is negligible. Therefore, parameters ψ_K and ψ_M are equal to zero. At the opposite, the braced framed in Figure

	Protection category			
	1		**2**	
	θ	μ	θ	μ
Reinforced concrete beams and slabs	$2° \simeq 35\,\mathrm{mrad}$	/	$4° \simeq 70\,\mathrm{mrad}$	/
Structural steel beams and plates	$2° \simeq 35\,\mathrm{mrad}$	10	$12° \simeq 210\,\mathrm{mrad}$	20

Table 1: Maximum values of ductility μ and rotation θ for steel and concrete structural elements according to two levels of protection defined by the US Army. [5]

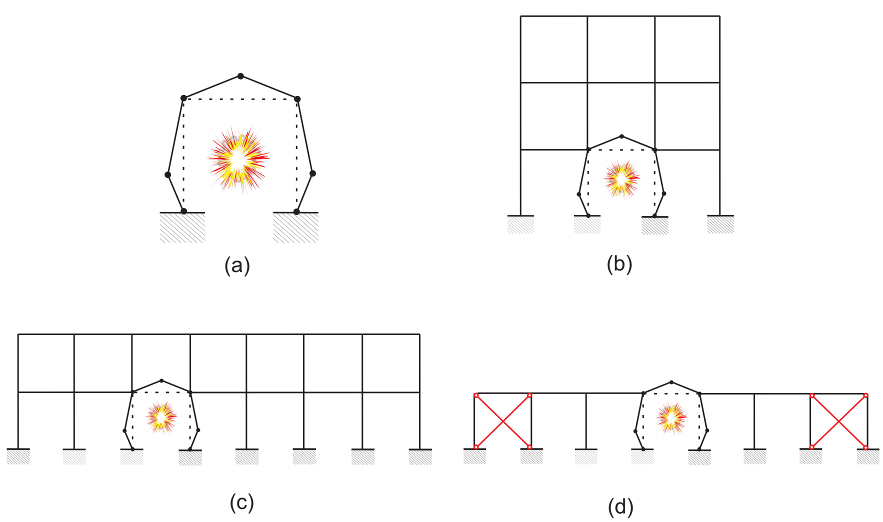

Figure 4: Steel structure configurations with IPE 270 beams ($5.4\,m$), HEA 240 columns ($4.5\,m$), CHS 175x5 braces and a linear mass of the floor equals to 2500 kg/m.

	Guyan condensation		Dynamic condensation		IRS		SEREP	
Structure	ψ_K [−]	ψ_M [−]	ψ_K [−]	ψ_M [−]	ψ_K [−]	ψ_M [−]	ψ_K [−]	ψ_M [−]
(b)	0.3	6.2	0.3	6.3	0.3	6.3	0.23	6.3
(c)	0.64	14.8	0.68	16.4	0.71	25.0	0.68	16.4
(d)	2.91	8.7	3.81	13.6	3.52	13.1	4.36	15.8

Table 2: Values of the dimensionless parameters ψ_K and ψ_M for different structures obtained by different reduction models.

4-d offers a large stiffness to the relative chord elongation of the beam. Of course, the more lateral columns and bracings, the more rigid the lateral restraint offered to the beam.

Table 2 gives the values of these parameters for the four structures illustrated in Figure 4. Since they immediately represent scaled versions of $K^\star$ and $M^\star$, which depend on the reduction technique, results obtained with the different reduction models are used. As expected, the Guyan (static) condensation is accurate for the assessment of the stiffness of the IAP of the structure but the inertia forces are not preserved. The IRS reduction process adjusts the Guyan condensation by adding some corrective terms so as to represent well the mass associated with the deleted DOF. For the dynamic condensation and the SEREP, one mode is needed to perform the reduction of the global model. This mode is selected such as it is the first mode that exhibits a relative horizontal displacement at the ends of the beam. These reduced models have the advantage to contain one natural frequency of the global model.

It should be noted that the Guyan process will be more appreciated if the IAP of the structure is loaded quasi-statically by the membrane force in the beam. Otherwise, the dynamic condensation or the SEREP are preferred. To cover a wide range of cases, the dimensionless parameter ψ_K and ψ_M are assumed to vary from 0 to 4 and from 0 to 20 respectively (in Figure 4).

The dimensionless parameters ξ and θ_y depend only on the properties of the profile and its span. Figure 5 represents, in a scatter plot, the relation between these two parameters according to the span-to-depth ratio of the beam for any class-1 S355 steel-grade steel profiles in the ArcelorMittal catalogue (such as I, H-shaped or tubular profiles). They are found to be inversely proportional to each other in the range of interest as indicated by the upper and lower envelopes represented by dashed lines. Indeed we observe that the dimensionless group

$$\xi\theta_y = \frac{1}{8}\frac{M_{pl}^2}{N_{pl}EI_b} \tag{37}$$

lies in the tiny range $[2.29\,10^{-4}; 2.63\,10^{-4}]$ for the (rather wide) set of considered steel profiles. The parameters ξ and θ_y vary from 4.2 % to 1.1 % and 6.2 mrad to 22 mrad respectively as the ratio $2\ell/h$ increases from 10 to 30 (Table 3).

Note that the dimensionless parameter ξ for the M-N interaction is analogous to the dimensionless parameter ν for the M-V interaction in [13], which is defined as a dimensionless ratio of the bending to shear strengths.

Three regimes can be observed according to the parameter τ_d, i.e. how fast the blasting develops according to the

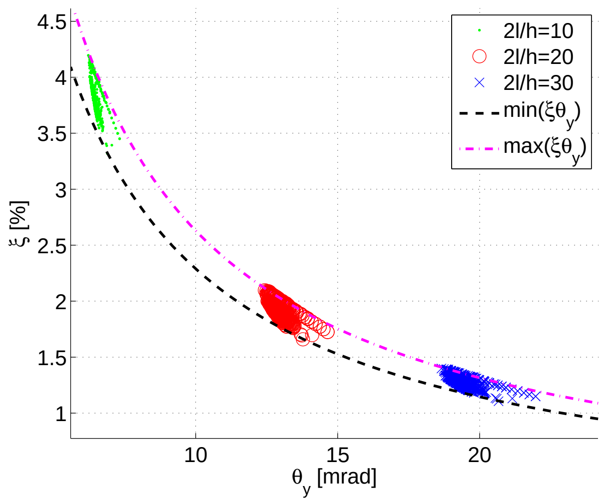

Figure 5: Relation between $\xi \times \theta_y$ for steel beams with S355 steel grade according to different ratios $2l/h$.

Ratio 2l/h	**10**	**20**	**30**
$min\,(\xi)$ [%]	3.3	1.7	1.1
$max\,(\xi)$ [%]	4.2	2.1	1.4
$min\,(\theta_y)$ [mrad]	6.2	12.4	18.7
$max\,(\theta_y)$ [mrad]	7.3	14.6	22

Table 3: Minimum and maximum values of the dimensionless parameters ξ [%] and θ_y [mrad] for steel beams with S355 steel grade according to different ratios $2l/h$.

natural timescale of the structure. For the impulsive ($\tau_d \ll 1$) and quasi-static ($\tau_d \gg 1$) regimes, some asymptotic analytical solutions are derived for the level of required ductility; they are provided in the following section. In the intermediate dynamic regime ($\tau_d \approx 1$), where the timescales of the loading and of the response interact, the set of equations (32), (34) and (35) must be solved.

3. Asymptotic Solutions

3.1. The quasi-static solution (p asymptote)

In the case of the quasi-static loading ($\tau_d \gg 1$), the terms involving velocity and acceleration in the equation of motion are discarded. From an energetic viewpoint, this corresponds to equating the work done by external forces to the strain energy stored in the structure [3]. In the quasi-static loading regime, the dimensionless work done by the blast loading until the maximum displacement is reached is

$$\overline{W} = \frac{W\left(X_m\right)}{2U_1\left(X_y\right)} = \frac{p_0 \ell X_m}{k_s X_y^2} \tag{38}$$

where we have taken $2U_1\left(X_y\right) = k_s X_y^2$ as a characteristic work. Furthemore, assuming $\beta = 1$ in order to develop (21) analytically, the dimensionless total strain energy at maximum displacement $\overline{U}_p$ reads

$$\overline{U}_p := \frac{U}{2U_1\left(X_y\right)} = \frac{1}{2} + \left[(\mu - 1) - \frac{\gamma}{\theta_y}\left(\Phi_{p,\alpha}\left(\mu\right) - \Phi_{p,\alpha}\left(1\right)\right)\right] + \frac{\psi_K \mu^4 \theta_y^2}{2} \tag{39}$$

with

$$\Phi_{p,\alpha}\left(\bar{X}\right) = \int_0^{\bar{X}} n\left(\overline{\chi}, 0, 0\right)^{\alpha} d\overline{\chi} = A_1^{\alpha} \frac{\bar{X}^{\alpha+1}}{(1+\alpha)} {}_2F_1\left(-\alpha; \alpha+1; \alpha+2; -\frac{A_2}{A_1}\bar{X}\right) \tag{40}$$

where $A_1 = 4\xi\theta_y$, $A_2 = 8\psi_K\xi\theta_y$ and ${}_2F_1\left(-\alpha; \alpha+1; \alpha+2; -\frac{A_2}{A_1}\bar{X}\right)$ is a hypergeometric function. In particular cases where $\alpha = 1$ or 2, the function $\Phi_{p,\alpha}\left(\bar{X}\right)$ simplifies into

$$\Phi_{p,1}\left(\bar{X}\right) = \left(\frac{A_2}{3}\bar{X}^3 + \frac{A_1}{2}\bar{X}^2\right) \quad ; \quad \Phi_{p,2}\left(\bar{X}\right) = \left(\frac{A_2^2}{5}\bar{X}^5 + \frac{A_1^2}{3}\bar{X}^3 + \frac{A_2 A_1}{2}\bar{X}^4\right). \tag{41}$$

Equating the dimensionless work in equation (38) to the dimensionless strain energy in equation (39) gives

$$\frac{p_0 \ell X_m}{k_s X_y^2} = \overline{U}_p\left(\mu, \psi_K, \xi, \theta_y\right) \tag{42}$$

or

$$\overline{p} := \frac{p_0}{p_s} = \frac{1}{\mu}\overline{U}_p\left(\mu, \psi_K, \xi, \theta_y\right). \tag{43}$$

This relation does not involve the momentum of the loading. This indicates that, in the quasi-static regime where inertial forces are neglected, the response μ only depends on the magnitude of the loading $\overline{p}$, not its duration. Consequently the level set representation of the ductility demand features horizontal asymptotes in the p-I diagram.

3.2. The impulsive solution (I asymptote)

At the fast timescale, for short duration of blasting compared to the natural period of the structure ($\tau_d \ll 1$), conservation of momentum over the short period of loading provides the initial structural velocity to be considered for the free response taking place after the loading has stopped. In this case, $\dot{X}_0 = I/M_s$ is the initial velocity at mid-span, since the additional mass M^* does not participate in the balance of momentum during this short loading phase, as the velocity $\dot{\delta}$ is proportional to the (small) generalized displacement X, see (6).

In the subsequent elastic-plastic free vibration problem, the maximum displacement is determined by equating the initial kinetic energy corresponding to this initial velocity and the strain energy in the system [3]. The initial dimensionless kinetic energy is given by

$$\overline{K}_0 := \frac{\frac{1}{2} M_s \dot{X_0}^2}{k_s X_y^2} = \frac{1}{2} \frac{I^2}{k_s M_s X_y^2}. \tag{44}$$

Thus, equating this dimensionless kinetic energy to the dimensionless strain energy gives

$$\frac{I^2}{k_s M_s X_y^2} = 2\overline{U}_I \left(\mu, \psi_K, \psi_M, \xi, \theta_y\right) \tag{45}$$

where the dimensionless total strain energy at maximum displacement $\overline{U}_I$ for impulsive loading can be written as below (assuming $\beta = 1$)

$$\overline{U}_I = \frac{U}{2U_1\left(X_y\right)} = \frac{1}{2} + \left[(\mu - 1) - \frac{\gamma}{\theta_y}\left(\Phi_I\left(\mu\right) - \Phi_I\left(1\right)\right)\right] + \frac{\psi_K \mu^4 \theta_y^2}{2} \tag{46}$$

with

$$\Phi_{I,\alpha}\left(\bar{X}\right) = \int_0^{\bar{X}} n\left(\overline{\chi}, \overline{\chi}', \overline{\chi}''\right)^\alpha d\overline{\chi} = \int_0^{\bar{X}} \left(4\xi\theta_y\overline{\chi} + 8\xi\theta_y\psi_K\overline{\chi}^2 + 4\psi_M\xi\theta_y\left(\overline{\chi}'^2 + \overline{\chi\chi}''\right)\right)^\alpha d\overline{\chi} \tag{47}$$

In case where $\beta \neq 1$, the expression for $\Phi_{I,\alpha}$ should be substituted with an appropriate numerical integration. The major difference between $\Phi_{I,\alpha}$ and $\Phi_{p,\alpha}$ concerns the consideration of the terms related to velocity and acceleration in the expression of the internal axial force.

Finally, the impulsive asymptote can be derived

$$\overline{I} := \frac{\overline{p}\tau_d}{2} = \frac{I}{\sqrt{k_s M_s} X_y} = \sqrt{2\overline{U}_I\left(\mu, \psi_K, \psi_M, \xi, \theta_y\right)} \tag{48}$$

where $\overline{I}$ is the dimensionless momentum associated with the blast loading. As this response does not depend on $\overline{p}$, the level set of the demand in ductility feature a vertical asymptote in the p-I diagram.

The integral in (47) is rather complex and requires, *a priori*, numerical integration. However, the function $\Phi_{I,\alpha}\left(\bar{X}\right)$ could be simplified. Observing that the transverse velocity $\bar{X}'$ varies from $\overline{I}$ to 0 as the displacement $\overline{X}$ increases from 0 to μ, we suggest to use the rough approximation

$$\bar{X}' \simeq \overline{I}\left(1-\frac{\bar{X}}{\mu}\right) \tag{49}$$

in order to simplify (47). This very simple model of the dynamics implies $\bar{X}=\mu\left(1-e^{-\overline{I}\tau/\mu}\right)$ which is quite far from the actual dynamics, especially in the fully elastic regime. However, we observe later that this assumption fits pretty well the elastic-plastic reponse.

Moreover, further assuming that $\overline{X}\ddot{\overline{X}} \ll \dot{\overline{X}}^2$, the function $\Phi_{I,\alpha}\left(\bar{X}\right)$ simplifies into

$$\Phi_{I,\alpha}\left(\bar{X}\right) \simeq \int_0^{\bar{X}} n\left(\overline{\chi},\dot{\overline{\chi}},\ddot{\overline{\chi}}\right)^{\alpha} d\overline{\chi} = \int_0^{\bar{X}} \left(A_1\overline{\chi}+A_2\overline{\chi}^2+A_3\left(1-\frac{\overline{\chi}}{\mu}\right)^2\right)^{\alpha} d\overline{\chi} \tag{50}$$

where $A_3 = 4\psi_M\xi\theta_y\overline{I}^2$. In particular cases such as $\alpha=1$ or 2, the function $\Phi_{I,\alpha}\left(\bar{X}\right)$ can be written as:

$$\Phi_{I,1}\left(\bar{X}\right) = \frac{A_2}{3}\bar{X}^3+\frac{A_1}{2}\bar{X}^2+\frac{A_3}{3\mu^2}\bar{X}^3-\frac{A_3}{\mu}\bar{X}^2+A_3\bar{X} \tag{51}$$

$$\begin{aligned}\Phi_{I,2}\left(\bar{X}\right) \quad = \quad & \frac{\bar{X}^3\left(A_1^2\mu^2-4A_1A_3\mu+2A_2A_3\mu^2+6A_3^2\right)}{3\mu^2}+\frac{\bar{X}^4\left(A_1\mu-2A_3\right)\left(A_2\mu^2+A_3\right)}{2\mu^3} \\ & -\frac{A_3\bar{X}^2\left(2A_3-A_1\mu\right)}{\mu}+\frac{\bar{X}^5\left(A_2\mu^2+A_3\right)^2}{5\mu^4}+A_3^2\bar{X}.\end{aligned} \tag{52}$$

Thus, the equation 48 becomes

$$\overline{I}^2 \simeq 2\overline{U}_I\left(\mu,\psi_K,\psi_M\overline{I}^2,\xi,\theta_y\right). \tag{53}$$

An iterative procedure should be used to obtain the impulsive solution. A first approximation of the solution can be obtained by neglecting the effects of the lateral inertia in equation 53, imposing therefore that $\psi_M=0$, in which case a simple analytical expression is obtained. A fixed point algorithm then provides a convenient recursive relation

$$\overline{I}^2_{(k+1)} \simeq 2\overline{U}_I\left(\mu,\psi_K,\psi_M\overline{I}^2_{(k)},\xi,\theta_y\right) \tag{54}$$

for the iterative correction of the first estimation.

4. Numerical Solutions

4.1. Description of the numerical method

The set of equations (32), (34) and (35) is solved with a nonlinear solver generalized from the high-order implicit scheme developed in [29].

4.2. Illustrative examples

Consider a structure composed by a steel beam IPE 270 with a S355 steel grade and a length $2\ell = 5.4\,m$. The linear mass of the reinforced concrete floor m_s is equal to $2500\,kg/m$. According to [18], the coefficients α, β and γ are chosen equal to $2, 1$ and 1 for strong axis bending. The safest approach proposed by the Eurocode 3 can also be used [19]. The peak overpressure and the positive phase duration of the blast loading are respectively equal to $306\,kN/m$ and $105\,ms$. The characteristic displacement, force and time are respectively $X_y = 0.034\,m$, $p_s\ell = 255\,kN$ and $T = 25\,ms$. They scale the results shown in Figure 5.

The dimensionless numbers of this problem obtained with a Guyan condensation of the IAP, as illustrated in Figure 4-c, are

$$\psi_K = 0.64\,;\ \psi_M = 14.8\,;\ \xi = 2\,\%\,;\ \theta_y = 13\,mrad\,;\ \overline{p} = 3.25\,;\ \tau_d = 5\,;\ \overline{I} = 8.125. \tag{55}$$

A value of τ_d close to 2π indicates that the duration of the loading is very similar to the natural period of the structure. The dimensionless pressure $\overline{p}$ larger than 0.5 indicates that some plasticity will develop. The objective is to determine the maximum displacement.

Figure 6-(a) illustrates the time evolution of the response. Figure 6-(b) shows the evolution of the internal forces in the force-displacement portrait. Four points labeled A, B, C and D describe the different stages of the response of the beam.

First, at point A, the plastic mechanism of the beam has just been formed, meaning that $\overline{X} = 1$. The sum of the internal forces is close to 1 since the effect of the lateral restraint is still negligible at this stage. At point B, the maximum dimensionless displacement (ductility demand) increases to 18.3, a bit after the moment where the blast loading stops. Between points A and B, the internal force in the beam first decreases as the membrane force increases. Then, it increases before reaching point B since the membrane force decreases because of the deceleration of the system, see (34). The internal force in the lateral restraint increases to reach a value close to the static plastic resistance of the beam.

After reaching the maximum displacement, the beam is subjected to an elastic unloading in the opposite direction. Indeed, the lateral restraint returns a part of its elastically stored energy to the beam. At point C, the plastic mechanism is developed in the opposite direction. Finally, at point D, the beam starts vibrating indefinitely elastically.

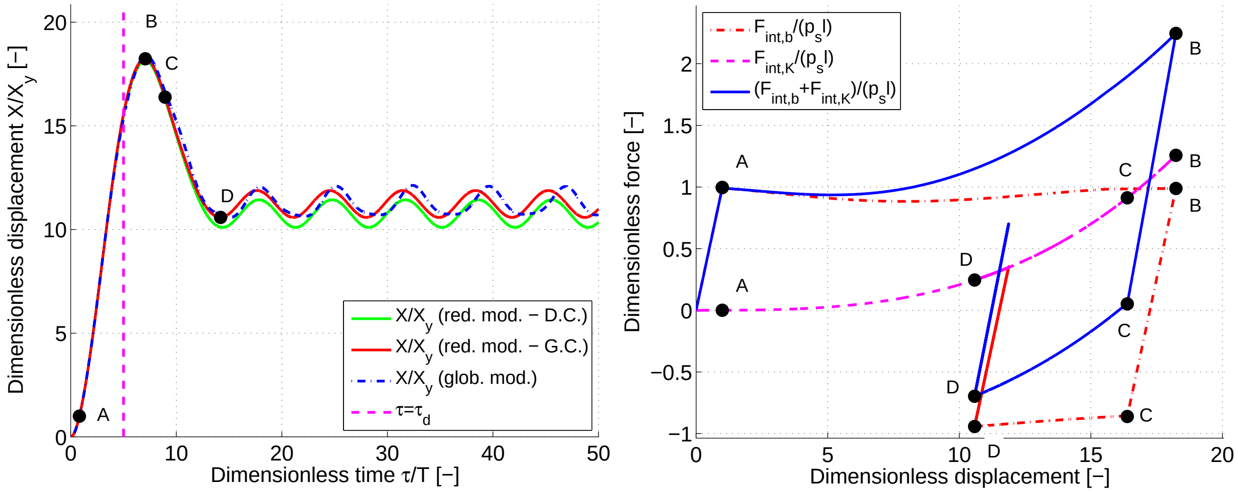

(a) (b)

Figure 6: (a) Displacement versus time – comparison between reduced and global models and (b) internal forces versus displacement for a given example considering the following parameters : $\psi_K = 0.64$; $\psi_M = 14.8$; $\xi = 2\,\%$; $\theta_y = 13\,mrad$; $\bar{p} = 3.25$; $\tau_d = 5$; $\bar{I} = 8.125$ (Guyan condensation).

The displacements of the beam obtained with reduced models, i.e. the Guyan condensation (G.C.) and the dynamic condensation (D.C.), seem to coincide as they provide values of ψ_K and ψ_M that are very close. Also, these curves fit well the dash-dot curve obtained by solving the multi-degree finite element model of the whole IAP of the structure. Each structural element of the IAP is modelled by two beam finite elements and the time step $d\tau$ is chosen as equal to $\tau_d/1000 = 5.10^{-3}$.

This detailed example corresponds to only one point in a (p-I) diagram, namely a required ductility of 18.3 for the couple $\left(\bar{p};\bar{I}\right) = (3.25; 8.125)$. This point is represented by a red dot in Figure 8-a.

For the braced structure (Figure 4-d), the values of the natural period T, the plastic resistance $p_s l$ of the beam as well as the blast loading does not change from the last example. Therefore, the structural parameters ξ and θ_y as well as the pressure and impulse of the blast loading $\left(\bar{p}, \bar{I}\right)$ are preserved. This modification is made on purpose in order to highlight the influence of parameters ψ_K and ψ_M only. The static response of the structure for the static condensation does not correspond exactly to the selected high-frequency mode shape of vibration used for the dynamic condensation, which results in a large discrepancy in values of the parameters ψ_K and ψ_M .

In Figure 7-a, the displacement shows the same behaviour until the first peak. However, the post-failure response computed with the dynamic condensation reduction technique is now different from the response obtained with the full finite element model of the structure, meaning that the response of the IAP of the structure is rather quasi-static than dynamic. Indeed, the IAP of the structure is loaded by the membrane force in the beam which is quasi-static as it mainly depends on the response of the beam and not directly on the blast loading. The braced system significantly mitigates the effect of the blast loading on the response of the beam thanks to its (elastic) stiffness; the maximum

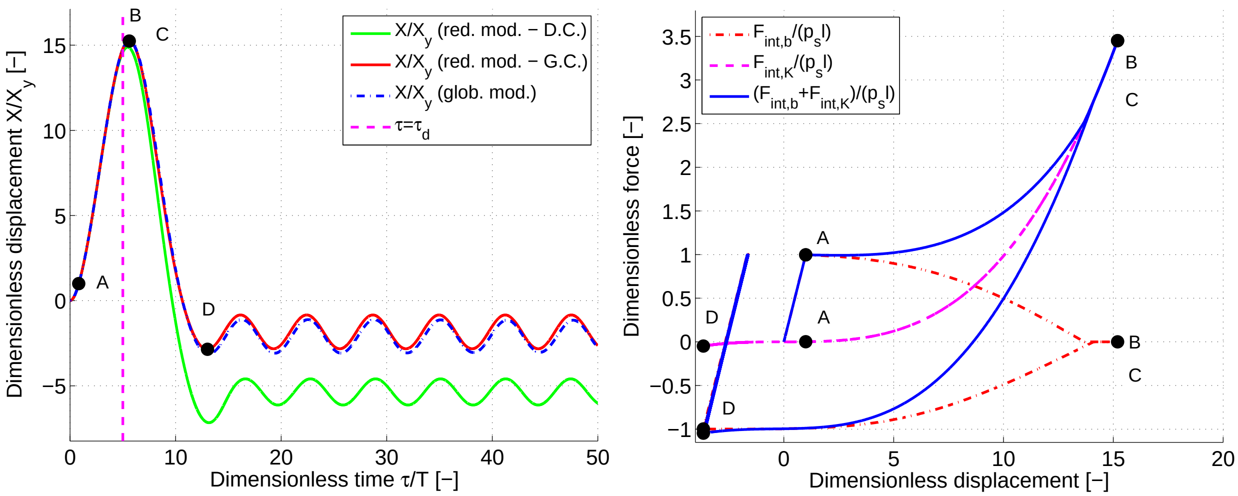

(a) (b)

Figure 7: (a) Displacement versus time – comparison between reduced and global models and (b) internal forces versus displacement for a given example considering the following parameters: $\psi_K = 2.91\,;\, \psi_M = 14.8\,;\, \xi = 2\,\%\,;\, \theta_y = 13\,mrad\,;\, \overline{p} = 3.25\,;\, \tau_d = 5\,;\, \overline{I} = 8.125$ (Guyan condensation)

displacement drops to 15.2 as shown in Figure 7-b.

5. Analysis of the Model

5.1. Influence of parameter ψ_K

In order to draw the p-I diagram, Krauthammer *et al.* developed three different search algorithms and presented their disadvantage in terms of the numerical stability, computational efficiency, generality of the method and compared the numerical results with tested structural elements [28]. Among these methods, it turns out that Blasko's procedure based on a polar coordinate system and the bissection method are appropriate for the needs of our study.

P-I diagrams are represented for $\psi_K = 0.64$ (Figure 8-a) and $\psi_K = 0$ (Figure 8-b), while other parameters are chosen as $\psi_M = 14.8\,;\, \xi = 2\,\%\,;\, \theta_y = 13\,mrad$. At a design stage, each curve represents the required ductility. The asymptotes represented with solid lines are obtained with the analytical procedures developed in Section 3; on the other hand, black dots are obtained with the numerical simulation of the governing equations of the problem. The good agreement between these results obtained with two different approaches, in the asymptotic cases, serves as a validation of the numerical code.

For a particular blast load ($\overline{p} = 3.25$, $\overline{I} = 8.125$), comparison of Figs. 8-a and 8-b shows that the required ductility is reduced from 23.7 to 18.3 when the lateral restraint is considered. The case $\psi_K = 0$ corresponds to an elastic-perfectly plastic beam model as the membrane force is negligible (the effect of ψ_M is much less influent when ψ_K is low). As a result, the quasi-static loading can not exceed the plastic resistance of the beam; in other words,

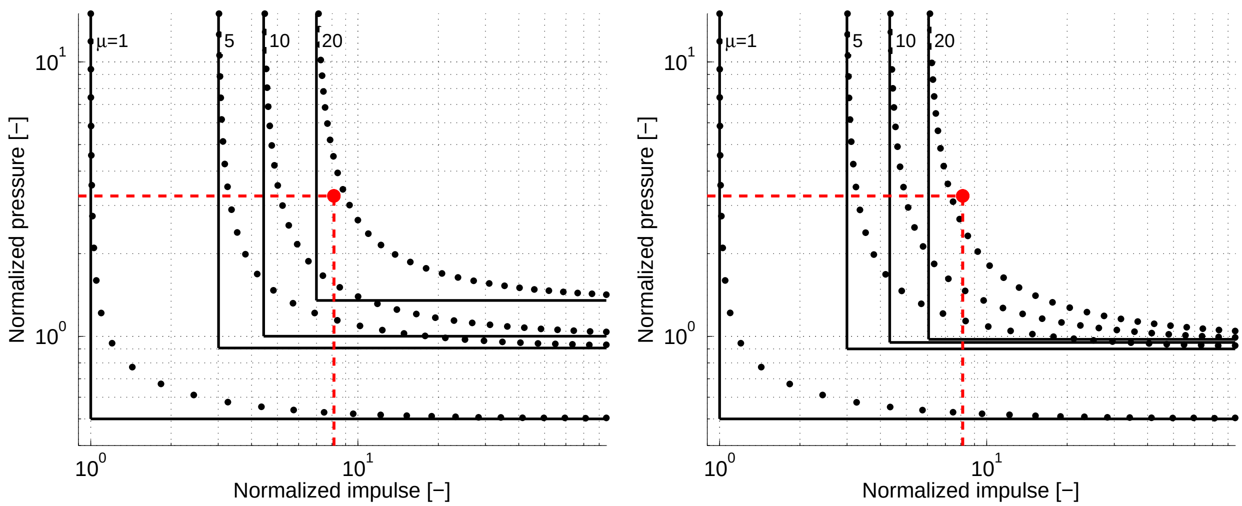

(a) (b)

Figure 8: Normalized p-I diagrams in logarithmic axes for (a) $\psi_K = 0.64$ and (b) $\psi_K = 0$. Other dimensionless parameters are ($\psi_M = 14.8\,;\,\xi = 2\,\%\,;\,\theta_y = 13\,mrad$).

the p-asymptote satisfies $\overline{p} < 1$. On the contrary, in the presence of a lateral restraint, the quasi-static asymptote might be significantly higher than $\overline{p} = 1$, and the lateral stiffness could therefore significantly affect the ductility demand for longer blast loads with smaller peak pressure.

Figure 9 illustrates the required ductility obtained with the analytical asymptotic approach as a function of parameter ψ_K ($\xi = 2\,\%$ and $\theta_y = 13$ mrad). It is represented as a function of (a) the dimensionless pressure in the quasi-static regimes and (b) of the dimensionless impulse in the impulsive regime. In Figure 9-(a), the curve AB corresponding to $\overline{p} = 1$ presents a vertical asymptote at $\psi_K = 0$. Indeed, for an elastic-perfectly plastic model, the ductility tends to infinity since the quasi-static loading approaches the plastic resistance; the only load that can be beared statically by the beam has to be smaller than $\overline{p} = 1$. For low blast loads, it is seen that the stiffness of the horizontal restraint has few influence on the required ductility. In fact the required ductility is so low that the transverse displacement of the beam is small and the membrane forces are almost not activated. On the contrary, Figure 9-(a) show that for large (quasi-static) blast loads the membrane action significantly reduces the required ductility. As to the impulsive asymptote, the lateral restraint is globally ineffective in contributing to the global resistance of the structure. One need a dimensionless impulse of more than $\overline{I} = 5$ to observe an influence on demand in ductility. This is explained, as discussed in Section 3.2, by the quadratic relation between the spring elongation and the transverse displacement of the beam. Notice that these influences on ψ_K on the asymptotic behaviours are also observable on the diagrams of Fig. (8).

For the first protection category ($\mu = 10$), the maximum acceptable blast loading can be increased up to $17\,\%$ and $7\,\%$ for quasi-static and impulsive loading respectively when the lateral restraint is taken into account. For the

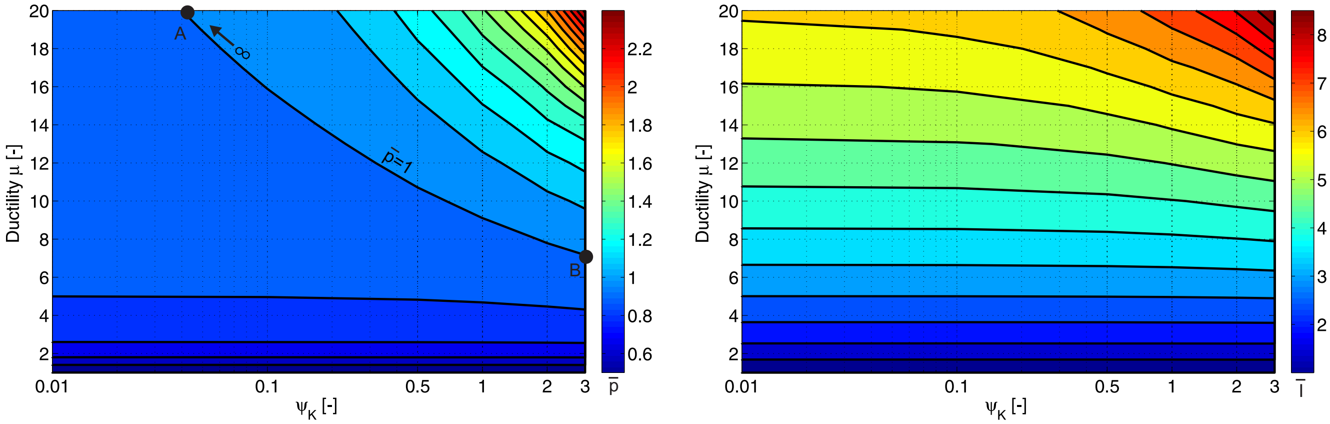

(a)

(b)

Figure 9: Required ductility ($\psi_M = 10\,;\, \xi = 2\,\%\,;\, \theta_y = 13\,mrad$ and ψ_K variable) (a) for dimensionless quasi-static loading $\overline{p}$ ($\tau_d \gg 1$) and (b) for dimensionless impulse loading $\overline{I}$ ($\tau_d \ll 1$).

second protection category ($\mu = 20$), these gains can reach up to 150 % and 50 % respectively.

5.2. The case of large membrane forces

Figures 10-a and -b illustrate, respectively, the structural behaviour of the SDOF model and the quasi-static asymptotic solution (see Equation (43)) for the following structural parameters $\psi_K = 3\,;\, \xi = 4\,\%\,;\, \theta_y = 7$ mrad. As the value of parameters ψ_K and ξ are high, the initial structural behaviour is an elastic-perfectly plastic softening model until the axial force in the beam resulting from the membranar restraint reaches the axial plastic resistance (Figure 10-a). At this last stage, the plastic hinges are fully articulated and the remaining resistance component in the SDOF model is the lateral restraint. The force-displacement response therefore features a slope discontinuity, see red dash-dot line, which translates into a similar discontinuity in the total internal force (in blue), which itself is however allowed to increase again owing to the elastic nature of the restraint. Because of this softening-hardening behaviour, equating the work of external forces and the strain energy stored in the structure present several solutions as shown in Figure 10-b where the vertical line at $\overline{p} = 0.9$ meets the quasi-static asymptotic solution at three points. In a "dynamic" step-by-step solution starting from initial conditions at rest, the physical solution is the first point of intersection between the vertical line and the quasi-static pressure curve since it would correspond to the first crossing, in time. A jump discontinuity is observed (from $\mu = 8$ to $\mu = 18$) for $\overline{p} = 0.94$; the equilibrium solution of the structure is unstable inbetween.

5.3. Assessment of the impulsive asymptotic solution

Equation (53) gives an analytical approximation of the required impulsive loading $\overline{I}_{app}$ to reach a given level of damage. In a design stage, this level of damage can be chosen as one of the target values corresponding to the two

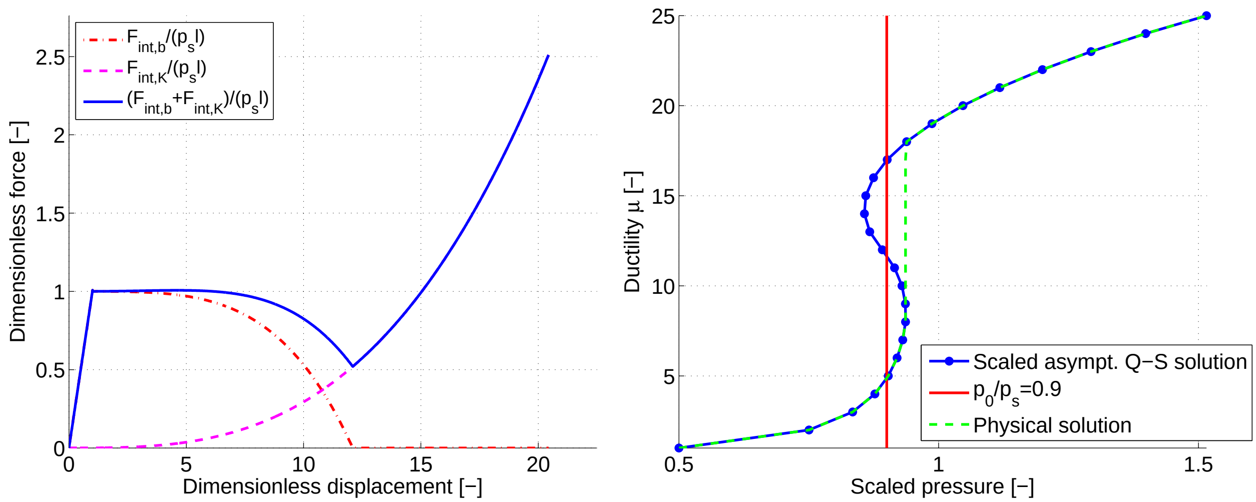

(a)

(b)

Figure 10: (a) Structural behaviour for $\xi = 4\,\%$; $\theta_y = 7\,mrad$ and $\psi_K = 3$; (b) Multiple solutions for a given quasi-static loading $\overline{p} = 0.9$.

levels of protection described in Table 1. The relative error of this approximation is defined as the following ratio $\left(\overline{I}_{act} - \overline{I}_{app}\right)/\overline{I}_{app}$ where $\overline{I}_{act}$ is the actual impulsive asymptote of the corresponding iso-damage curve of the p-I diagram.

All the dimensionless parameters are taken trough their practical range, the parameter ψ_K varies from 0 to 3 and the other parameters ξ and θ_y are approximately the mean values of range boundaries for three different ratios of $2l/h$ detailed in Table 3. The last parameter ψ_M takes its maximum value, i.e. 20, corresponding to the highest level of error.

For the first category of protection, the relative error is less than $1.5\,\%$ (figure 11-a). However, for the second category of protection, the relative error reaches a maximum value of about $6\,\%$ (figure 11-b).

5.4. Influence of parameters ξ and θ_y

The effect of parameters ξ and θ_y on the p-I diagram is illustrated in Figure 12, for $\psi_K = 1$ and $\psi_M = 10$. The two parameters are not varied independently, but well along the hyperbola of high correlation disclosed in Fig. 5. If the beam span-to-depth ratio is increased ($\xi \downarrow$ and $\theta_y \uparrow$), the energy dissipated in the plastic hinges is reduced. As a result, the lateral mass and restraint should contribute more to dissipation of the energy generated by the blast loading. Therefore, the required ductility decreases, see Figure 12-a, as the lateral force, which is a cubic function of the displacement, increases rapidly.

Same conclusions hold if the bending properties are constant and the beam axial plastic resistance is decreased ($\xi \uparrow$ and θ_y constant).

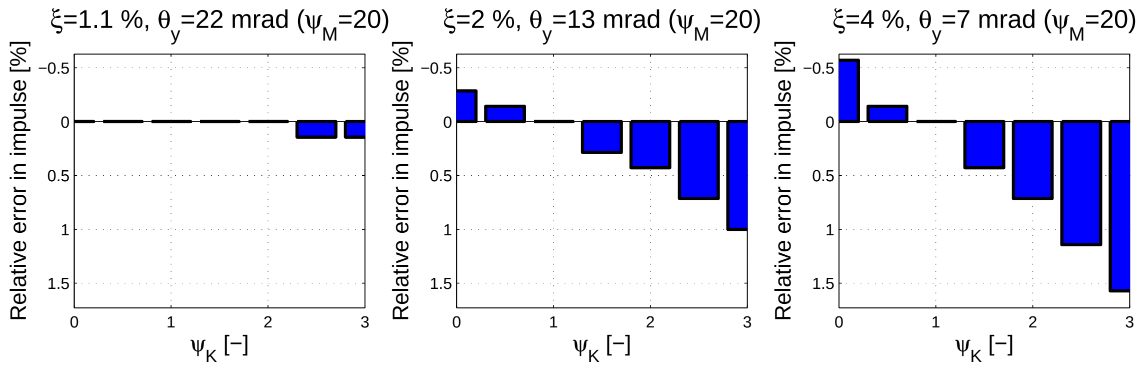

(a)

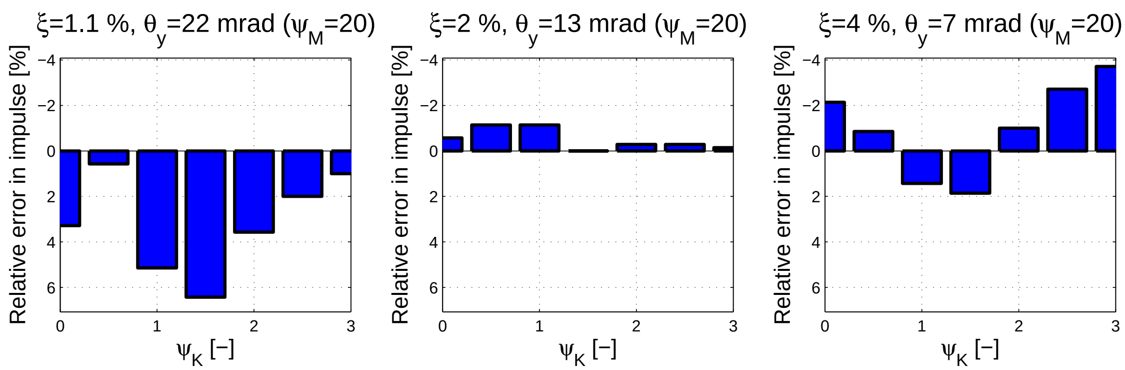

(b)

Figure 11: Relative error in the assessment of the impulsive asymptotic solution for variable dimensionless parameters (a) for first and (b) second category of protection.

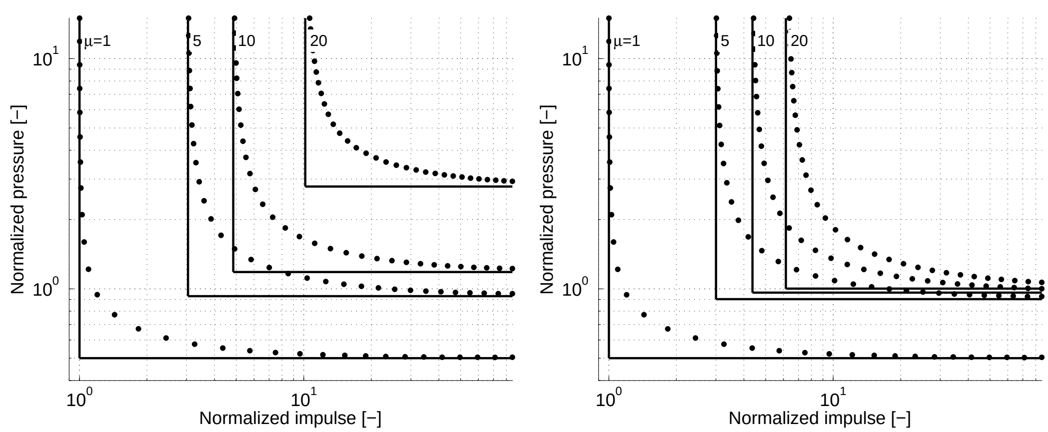

(a) (b)

Figure 12: Normalized p-I diagrams in logarithmic axes for $\psi_K = 1$, $\psi_M = 10$ (a) $\xi = 1.1\,\%$, $\theta_y = 22\,mrad$ and (b) $\xi = 4\,\%$, $\theta_y = 7\,mrad$.

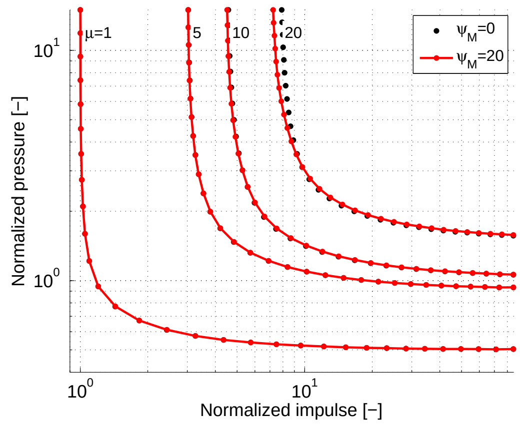

Figure 13: Comparison of normalized p-I diagrams in logarithmic axes for $\psi_K = 1$, $\xi = 2\,\%$, $\theta_y = 13\,mrad$, $\psi_M = 0$ and $\psi_M = 20$.

5.5. *Influence of parameter* ψ_M

With the help of numerical step-by-step simulations, it is found that the participating mass $M^\star$ does not affect significantly the response. It has strictly no influence in the quasi-static regime, as expected. In the impulsive regime, these numerical simulations reveal that parameter ψ_M does not affect significantly the response for ductilities lower than 10, see Figure 13, but well for required ductilities of about 20, where an influence of up to 8 % might be observed. Upon varying the values of other parameters in their practical range of interest, the maximum relative error might reach 12 %.

6. Conclusions

The considered problem is that of a frame beam subjected to blast loading considering the interaction with the indirectly affected part of the structure. The purpose is to establish the p-I diagram for a beam extracted from an arbitrary structure (such as a steel, concrete and composite structures) taking into account the nonlinear membrane force, the M-N interaction and the lateral inertia and restraint provided by the rest of the structure.

As a result of the dimensionless analysis, four dimensionless structural parameters affecting the required ductility of the frame beam are identified. Two parameters ψ_K and ψ_M are related to the behaviour of the indirectly affected part (the lateral restraint and mass). Another one ξ is related to the mechanical properties of the investigated beam (i.e. its bending and axial resistances). The last parameter θ_y is related to the kinematic of the problem (i.e. the yield rotation of the beam at its extremities).

Parameter ψ_K outlines the favourable effect of the elastic indirectly affected part of the structure to limit the required ductility of the frame beam. If the beam span-to-depth ratio is increased ($\xi \downarrow$ and $\theta_y \uparrow$), the energy dissipated in the plastic hinges is reduced. Thus, the lateral mass and restraint should contribute more to absorb the energy generated by the blast loading and reduce the demand of ductility. Parameter ψ_M influences the impulsive regime of the p-I diagrams for the second category of protection. The relative error made if this parameter is not taken into account can reach up to 12 %.

[1] B. Li, T. Pan, and A. Nair, “A case study of the structural responses of a tall building in Singapore subjected to close-in detonations,” vol. 246, no. July 2009, pp. 223–246, 2011.

[2] L. Comeliau, B. Rossi, and J.-F. Demonceau, “Robustness of steel and composite buildings suffering the dynamic loss of a column,” Struct. Eng. Int., vol. 22, no. 3, pp. 323–329, 2012.

[3] J. G. Hetherington and P. D. Smith, Blast and Ballistic Loading of structures. Oxford: Elsevier Science, 1994.

[4] G. C. Mays and P. D. Smith, Blast effects on buildings: Design of buildings to optimize resistance to blast loading. Thomas Telford, 1995.

[5] W. E. Baker, P. A. Cox, J. J. Kulesz, R. A. Strehlow, and P. S. Westine, Explosion hazards and evaluation. Access Online via Elsevier, 1983.

[6] US Army, “Structures to resist the effects of accidental explosions.” TM5-1300, 1990.

[7] Y. Shi, H. Hao, and Z.-X. Li, “Numerical derivation of pressure–impulse diagrams for prediction of RC column damage to blast loads,” International Journal of Impact Engineering, vol. 35, no. 11, pp. 1213–1227, Nov. 2008.

[8] H. C. Yim and T. Krauthammer, “Mechanical properties of single-plate shear connections under monotonic, cyclic, and blast loads,” Engineering Structures, vol. 37, pp. 24–35, Apr. 2012.

[9] N. Jones, Structural impact. Cambridge University Press, 2011.

[10] Q. M. Li and N. Jones, “Blast Loading of Fully Clamped Beams with Transverse Shear Effects,” J. Struct. Mech., vol. 23, no. 1, pp. 59–86, 1995.

[11] Li, Q. M., & Jones, N. (1999). Shear and adiabatic shear failures in an impulsively loaded fully clamped beam. International Journal of Impact Engineering, 22(6), 589–607.

[12] Y. H. Liang, L. a. Louca, and R. E. Hobbs, “Corrugated panels under dynamic loads,” Int. J. Impact Eng., vol. 34, no. 7, pp. 1185–1201, Jul. 2007.

[13] G. W. Ma, H. J. Shi, and D. W. Shu, “P–I diagram method for combined failure modes of rigid-plastic beams,” Int. J. Impact Eng., vol. 34, no. 6, pp. 1081–1094, Jun. 2007.

[14] Vaziri, R., Olson, M. D., & Anderson, D. L. (1987). Dynamic response of axially constrained plastic beams to blast loads. International journal of solids and structures, 23(1), 153-174.

[15] G. S. Langdon and G. K. Schleyer, “Inelastic deformation and failure of profiled stainless steel blast wall panels. Part II: analytical modelling considerations,” Int. J. Impact Eng., vol. 31, no. 4, pp. 371–399, Apr. 2005.

[16] A. S. Fallah and L. A. Louca, “Pressure–impulse diagrams for elastic-plastic-hardening and softening single-degree-of-freedom models subjected to blast loading,” Int. J. Impact Eng., vol. 34, no. 4, pp. 823–842, Apr. 2007.

[17] J. Dragos and C. Wu, “A new general approach to derive normalised pressure impulse curves,” Int. J. Impact Eng., vol. 62, pp. 1–12, Dec. 2013.

[18] M. Villette, Critical analysis of the treatment of members subjected to compression and bending and propositions of new formulations (in French). Phd Thesis. Liege University, 2004.

[19] European comittee for standardization, “EN 1993-1-1. Eurocode 3: Design of steel structures - Part 1-1: General rules and rules for buildings,” 2005.

[20] Bentz, “Response-2000 program.” http://www.ecf.utoronto.ca/˜bentz/r2k.htm (last accessed in May 2014), 2000.

[21] J.-F. Demonceau, J.-P. Jaspart, R. Klinkhammer, R. Oerder, K. Weynand, F. Labory, and L.-G. Cajot, “Recent developments in composite connections,” Steel Constr., vol. 1, no. 1, pp. 71–76, Sep. 2008.

[22] J.-F. Demonceau and J.-P. Jaspart, “Experimental and analytical investigations on the response of structural building frames further to a column loss” Proceedings of the Structures Congress, 2009, pp. 1801–1810.

[23] R. J. Guyan, “Reduction of stiffness and mass matrices,” AIAA J., vol. 3, no. 2, p. 380, Feb. 1965.

[24] C. Flanigan, “Implementation of the IRS dynamic reduction method in MSC/NASTRAN,” in 1990 MSC/Nastran World Users Conference, 1990.

[25] N. Zhang, “Dynamic condensation of mass and stiffness matrices,” J. Sound Vib., vol. 188, no. 4, pp. 601–615, 1995.

[26] M. Papadopoulos and E. Garcia, “Improvement in model reduction schemes using the system equivalent reduction expansion process,” AIAA J., vol. 34, no. 10, pp. 2217–2219, 1996.

[27] N. M. Newmark, “A Method of Computation for Structural Dynamics,” J. Eng. Mech. Div. (ASCE),85,EM3, pp. 67–94, 1959.

[28] T. Krauthammer, S. Astarlioglu, J. Blasko, T. B. Soh, and P. H. Ng, “Pressure–impulse diagrams for the behavior assessment of structural components,” Int. J. Impact Eng., vol. 35, no. 8, pp. 771–783, Aug. 2008.

[29] A. Depouhon, E. Detournay, and V. Denoël, “Accuracy of one-step integration schemes for damped/forced linear structural dynamics,” Int. J. Numer. Methods Eng., vol. 99, no. 5, pp. 333–353, Aug. 2014.